JOURNAL OF GEOPHYSICAL RESEARCH, VOL. 108, NO. D9, 4279, doi:10.1029/2002JD002998, 2003

Humidity-dependent optical properties of fine particles during the Big Bend Regional Aerosol and Visibility Observational Study

William C. Malm

National Park Service-Air Resources Division, Cooperative Institute for Research in the Atmosphere, Colorado State University, Fort Collins, Colorado, USA

Derek E. Day

Cooperative Institute for Research in the Atmosphere, Colorado State University, Fort Collins, Colorado, USA

Sonia M. Kreidenweis, Jeffrey L. Collett, and Taehyoung Lee

Department of Atmospheric Science, Colorado State University, Fort Collins, Colorado, USA

Received 30 September 2002; revised 18 December 2002; accepted 7 January 2003; published 10 May 2003.

[1] The Environmental Protection Agency (EPA) and National Park Service (NPS) initiated a comprehensive field experiment called The Big Bend Regional Aerosol and Visibility Observational Study (BRAVO) to investigate the source of visibility-reducing aerosols at Big Bend National Park, Texas. The study was carried out over a period of 4 months starting in the first week of July 1999. One objective of the study was to gain insight into the atmospheric light-scattering properties of ambient aerosols, especially as they relate to their hygroscopicity. This paper will report on comparisons between measured and modeled estimations of dry and ambient scattering and comparisons between measured and modeled ratios of wet and dry scattering, *f*(RH), as a function of relative humidity (RH). Two equilibrium models, exercised in combination with Mie scattering theory, were used to predict atmospheric aerosol water content and associated increase in atmospheric scattering. Modeled and measured deliquescence and crystallization points were also compared. Measured and modeled deliquescence were always within 10% RH while crystallization RHs were always within a few percentage points. The analysis suggests that on most days some water is retained by the aerosol at low RHs (20–30%) and in most cases the hygroscopic growth of only inorganic salts accounted for all the observed increase in scattering as a function of RH. *INDEX TERMS:* 0305 Atmospheric Composition and Structure: Aerosols and particles (0345, 4801); 0335 Atmospheric Composition and Structure: Ion chemistry of the atmosphere (2419, 2427); 0340 Atmospheric Composition and Structure: Middle atmosphere—composition and chemistry; *KEYWORDS:* hygroscopicity, scattering, extinction, aerosols, visibility, sulfates

Citation: Malm, W. C., D. E. Day, S. M. Kreidenweis, J. L. Collett, and T. Lee, Humidity-dependent optical properties of fine particles during the Big Bend Regional Aerosol and Visibility Observational Study, *J. Geophys. Res.*, *108*(D9), 4279, doi:10.1029/2002JD002998, 2003.

1. Introduction

[2] Haze and related species concentrations have increased over the last decade in West Texas and southern New Mexico [*Malm et al.*, 2000b, 2002]. To investigate the sources of emissions associated with this increase, the Environmental Protection Agency (EPA) and National Park Service (NPS) initiated a field experiment referred to as The Big Bend Regional Aerosol and Visibility Observational Study (BRAVO). The study was carried out over a period of 4 months starting in the first week of July 1999.

[3] The overall goal of the study was to apportion the major aerosol species to their emission sources, with secondary goals of understanding the physio/chemical/optical properties of aerosols, especially as they relate to their hygroscopicity. This paper will focus on the skill of models in predicting dry and ambient particle scattering, including predicting measured ratios of wet to dry scattering, *f*(RH), of ambient aerosols as a function of relative humidity (RH).

[4] Detailed chemical composition was measured in the fine (0.0–2.5 μm, $PM_{2.5}$) and coarse (2.5–10.0 μm, PM_{10}-$PM_{2.5}$) modes using the Interagency Monitoring of Protected Visual Environments (IMPROVE) sampling system, as well as in eight size ranges using the Micro Orifice Uniform Deposit Impactor (MOUDI). Ions, elements, and organic and elemental carbon were measured with the IMPROVE system [*Malm et al.*, 1994], while only inorganic ions were analyzed from the MOUDI substrates. Optical measurements were made with ambient-integrating

0148-0227/03/2002JD002998$09.00

nephelometers, one of which was fitted with a cyclone inlet (admitting particles with aerodynamic diameters <2.5 μm), another with a PM_{10} inlet, and a third in the "open air" configuration. The hygroscopic properties of ambient particles were examined using a humidograph with the ability to measure scattering as a function of humidity over ranges of about 15–95%. *Day et al.* [2000] described the instrument design in some detail and therefore its operation will only be summarized here. Fine particle absorption estimates were made with an aethalometer and from measurements of elemental carbon.

[5] Experiments were designed such that observables could be estimated or modeled in a number of different ways. Mass was gravimetrically determined for both D_{aero} < 10 and 2.5 μm, which can be compared to reconstructed mass based on measured aerosol species. Dry and ambient scattering coefficients were measured, which in turn can be compared to modeled scattering coefficients that are based on aerosol species mass and size measurements. Humidograph measurements of scattering coefficients as functions of RH can be compared to modeled scattering coefficients that include thermodynamic model predictions of inorganic aerosol hygroscopic growth.

[6] Previous studies of aerosol hygroscopicity have been made using Tandem Differential Mobility Analyzers (TDMA) and have been summarized in the work of *Cocker et al.* [2001]. Most studies used humidification ranges of 80–90%. A number of these studies reported two growth modes: a less hygroscopic mode with growth factors of 1.0–1.4 and a more hygroscopic mode with growth factors as high as 1.8. In chamber studies, *Virkkula et al.* [1999] reported a growth factor of about 1.1 for a no-seed secondary organic case and a growth factor starting at 1.5 for an ammonium sulfate seed, but dropping to 1.1 near the end of the experiment. The affinity of organic compounds for water, particularly those organic species found in the ambient atmosphere, is not as well characterized, despite the fact that these species often account for a significant amount of the total fine mass in continental aerosols [*Malm et al.*, 1994]. As reviewed by *Saxena and Hildemann* [1996], organic particulate matter contains hundreds of compounds, spanning a range of carbon numbers, functional groups, and solubility in polar and nonpolar solvents.

[7] Measurement of particle scattering as a function of RH was pioneered by *Covert et al.* [1979] and *Waggoner et al.* [1983]. They made limited measurements at a number of locations including Tyson, Missouri, Point Reyes, California, Shenandoah National Park, and Houston, Texas. *Malm and Day* [2001] reported on measurements of the RH enhancement factor which is defined to be the ratio of the scattering coefficient at some RH divided by the scattering coefficient at some minimum RH ($f(RH) = b_{scat}(RH)/b_{scat}(RH_{min})$). Measurements were carried out at Great Smoky Mountains and Grand Canyon National Parks. The $f(RH)$ function was smoothly increasing as a function of increasing RH for both data sets. However, for the most part, the $f(RH)$ at Great Smoky Mountains began to increase at relative humidities just above 20%, while at Grand Canyon increases did not take place until approximately 40–45%, and in some cases not until 60%. At Grand Canyon, the $f(RH)$ was more varied than at Great Smoky Mountains. For instance, in the range of 80–85% RH the $f(RH)$ values varied between 1.53 and 2.75 at Great Smoky Mountains, while at Grand Canyon the range was from near 1 to 4.0. In general, as the contributions of organics and soil dust to mass concentration increase, the increase of $f(RH)$ with humidity decreases. Growth factors and ambient light-scattering efficiencies have previously been observed to be rather smooth functions of RH [*Sloane*, 1986; *Malm et al.*, 2000a]. Measurements of $f(RH)$ at coastal sites in Tasmania and Portugal showed qualitatively similar results in which pollution dominated aerosols showed smoothly varying $f(RH)$, though marine dominated aerosols showed strongly deliquescent and more hygroscopic $f(RH)$ [*Carrico et al.*, 1998, 2000]. *Rood et al.* [1989] showed evidence for the existence of metastable aerosol in the ambient atmosphere. Differences in measurements of $f(RH)$ between the deliquescence and crystallization branches were ~10% on average for polluted aerosols and ~20% on average for marine aerosols, though it is as much as 50% for individual RH scans [*Carrico et al.*, 2000].

[8] A variety of scattering models were used in an attempt to reproduce measured $f(RH)$ curves. At Great Smoky Mountains, both internally and externally mixed aerosol models were used assuming the measured sulfate ion was fully neutralized, and assuming variable degrees of neutralization corresponding to the measured ammonium ion concentrations and with and without accounting for sampling-period-to-sampling-period shifts in size distribution [*Malm et al.*, 2000a]. The model sensitivity in using the deliquescence and crystallization branches, as well as a curve smoothed between the deliquescence and crystallization points of D/D_o curves as a function of RH for inorganic salts, was also explored. Scattering coefficient predictions as a function of RH were most sensitive to the assumptions regarding sulfate ammoniation and the smoothed D/D_o growth curves. Changes in $f(RH)$ as a function of assumptions concerning mixing were less than 10% on the average.

[9] For the analysis of the data from Grand Canyon [*Malm and Day*, 2001], only the externally mixed model was used; sulfate was assumed to be in the form of ammonium sulfate, and a smoothed $f(RH)$ curve was used based on size distribution measurements made in previous studies. At Grand Canyon the assumptions of constant mass scattering efficiencies, complete sulfate ammoniation, and a constant $f(RH)$ yielded, on an average, very reasonable results. However, on some days parts of the measured and predicted $f(RH)$ curves varied by as much as ±20%. An Ordinary Least Squares (OLS) regression between measured and predicted $f(RH)$ values yielded an $R^2 = 0.82$ with a slope of 1.02 ± 0.006 when the intercept term was forced through zero. The implication is that, on the average, predicted $f(RH)$ values were about 2% greater than measured. The results of both the Grand Canyon and Great Smoky Mountains studies suggested that organic aerosols were weakly hygroscopic or nonhygroscopic.

[10] In this paper we will further explore what influence particle size distribution, the degree of sulfate ammoniation, and chemical composition have on aerosol scattering as a function of RH. Two equilibrium models, ISORROPIA [*Nenes et al.*, 1998] and the Aerosol Inorganics Model (AIM), [*Clegg et al.*, 1992, 1998b] are used to estimate inorganic aerosol growth. Specifically, we will compare measured $f(RH)$ curves to modeled curves assuming water

contents based on both the deliquescence and crystallization branches of the thermodynamic diagrams. We will evaluate the ability of equilibrium models to predict crystallization or deliquescence where it is observed, and finally, we will compare the ability of scattering models to predict measured *f*(RH) curves as a function of equilibrium modeling assumptions, hygroscopicity of aerosol species other than inorganic salts, and aerosol size distributions.

2. Experimental Methods

2.1. Integrating Nephelometers

[11] The details of ambient nephelometer measurements were covered in the work of *Malm et al.* [1994], *Molenar* [1997], *Malm and Day* [2000], and *Day et al.* [2000] and will only be briefly reviewed here. Five Optec NGN-2 integrating nephelometers, in various configurations, were operated during the study. One nephelometer was fitted with an Anderson PM_{10} inlet, while two Optec nephelometers were operated at reduced flow rates (113 l min^{-1}) and were fitted with a Bendix-240 cyclone inlet with a 2.5 μm cutpoint. Two nephelometers utilized the open-air configuration and were operated using standard IMPROVE protocols [*Air Resource Specialists*, 1995]. Thermistors were placed inside the inlet, where sample air was assumed to be at ambient temperature, and at the sample exit, where sample air temperature should have reflected any heating of the aerosol. Monitoring the difference in sample temperature between the inlet and the outlet of each nephelometer allowed determination of whether heating of the sample had occurred and if there was a subsequent change in sample RH. Generally, the degree to which the sample was heated was less than 0.5°C. The accuracy of the nephelometer measurements in this configuration and the degree of heating were discussed in some detail by *Day et al.* [2000].

[12] A sixth and seventh nephelometer (Radiance Research M903 integrating nephelometers) were configured to measure dry and controlled humidity (D_{aero} < 2.5 mm) scattering. In the controlled humidity configuration, prior to measurements by the nephelometer, air was drawn through a temperature-controlled humidity conditioner consisting of Perma Pure Nafion dryers, while temperature was controlled by placing the dryers in a constant temperature water bath. Because temperature changes in the sampling plumbing can cause unwanted and unknown RH changes, temperatures were monitored throughout the system.

2.2. Relative Humidity Sensors

[13] Three Rotronics mp 100f combination RH/temperature sensors were housed in PVC holders and aspirated by a fan. The reported accuracy of the RH sensor is ±2%. The flow rate through the holder was approximately 120 l min^{-1}. The sensors were approximately 3 m above ground level, 3 m from each other, and mounted near the inlets of the nephelometers.

2.3. Particulate Samplers

[14] The IMPROVE sampler was designed for the IMPROVE network and has been operated extensively in the network and during field studies since 1988 [*Malm et al.*, 1994]. The IMPROVE sampler consists of three independent modules for monitoring fine particles and a fourth module is used to collect particles that are less than 10 μm. Each module incorporates a separate inlet array, filter pack, and pump assembly; however, all modules are controlled by one timing mechanism. It is convenient to consider a particular module, its associated filter, and the parameters measured from the filter as a channel of measurement (i.e., channel A).

[15] Channels A, B, and C are each equipped with a 2.5 μm cyclone inlet. Channel A, which utilizes a Teflon filter, was analyzed for fine mass ($PM_{2.5}$) gravimetrically, nearly all elements with atomic mass number >11 (Na) and <82 (Pb) by proton induced X-ray emission (PIXE) and by X-ray florescence (XRF), elemental hydrogen by proton elastic scattering analysis (PESA), and light absorption.

[16] Channel B utilizes a single Nylasorb filter as a collection substrate. The material collected on the filter was extracted ultrasonically in an aqueous solution that was subsequently analyzed by ion chromatography for the anions sulfate, nitrate, nitrite, and chloride. Sodium, ammonium, potassium, magnesium, and calcium ion concentrations were also measured using extracts from these filters.

[17] Channel C utilizes tandem quartz fiber filters for the collection of fine particles and the estimation of the organic carbon artifact from organic gases collected on the secondary filter. These filters were analyzed by thermal optical reflectance (TOR) for elemental and organic carbon [*Chow et al.*, 1993].

[18] Additional channel A, B, and C samplers were run with PM_{10}, rather than with $PM_{2.5}$, inlets so that coarse particle species mass concentrations could be estimated by differencing PM_{10} and $PM_{2.5}$ concentrations. The 24-hour filter samples were collected each day starting at 0800 hours. Exposed cassettes from channels A, B, and C were stored in sealed plastic bags and shipped for storage and analysis.

[19] A URG annular denuder/filter pack system was used to collect daily 24-hour samples of $PM_{2.5}$ as well as gaseous ammonia and nitric acid. The system consisted of the following components, arranged in series: cyclone with size cut of 2.5 μm aerodynamic diameter, 242 mm glass annular denuder coated with NaCl for nitric acid collection, 242 mm glass annular denuder with a citric acid coating to collect ammonia, 47 mm Teflon filter (Gelman Teflo, 2 μm pore size) for particle collection, and 47 mm nylon filter (Gelman Nylasorb) for collection of nitrate lost by volatilization from the Teflon filter. Air was drawn through the sampler at 10 l min^{-1}, with mass flow control. Sampling volumes were verified using an in-line dry gas meter.

[20] Twenty-four hour size-resolved particle measurements were made using a MOUDI [*Marple et al.*, 1991] sampler, and greased aluminum impaction substrates were analyzed by ion chromatography for the same ions as discussed earlier. Size ranges were >18.0, 10.0–18.0, 5.6–10.0, 3.2–5.6, 1.8–3.2, 1.0–1.8, 0.56–1.0, 0.32–0.56, and 0.18–0.32 μm. All sample inlets were operated at ambient RH.

3. Determination of Aerosol Types

[21] The fine aerosol species at most continental sites can be classified into five major types: sulfates, nitrates, organics, light-absorbing carbon, and soil. Other fine species such

Table 1. Statistical Summary of Concentrations of Selected Ions as Measured Using the MOUDI Sampler[a]

Ions, nmol m^{-3}	Mean	Standard Deviation	Minimum	Maximum
Sulfate	29.79	27.01	4.11	94.57
Ammonium	42.85	33.74	7.10	122.86
Nitrate	6.87	3.80	1.25	19.36
Sodium	5.92	5.76	0.04	21.83

[a]Concentrations are presented in terms of nanomoles. The number of samples is equal to 40.

as nonsoil potassium, sea salt, and other trace elements are less important from a visibility standpoint. Details of standard methods for apportionment of measured mass to the various aerosol species are described in some detail in the work of *Malm et al.* [1994].

[22] An average ambient particulate organic compound was assumed to have a constant fraction of carbon by weight. Organic carbon mass concentration (OMC) from channel C was assumed to be [OMC] = 1.4[OC]. The factor of 1.4 corrects the organic carbon mass for other elements associated with an assumed average organic molecular composition [*White and Roberts*, 1977]. However, *Turpin and Lim* [2001] suggest that this factor could be as high as 2.1. Elemental carbon (EC) was also obtained from TOR analysis.

[23] Soil mass concentration (SOIL) was estimated by summing the elements predominantly associated with soil plus oxygen for the common compounds (Al_2O_3, SiO_2, CaO, K_2O, FeO, Fe_2O_3, TiO_2) and applying a correction for other compounds such as MgO, Na_2O, water, and carbonate.

[24] Aerosol species distributions were measured using an eight-stage MOUDI sampler and, on 41 of the 125 sampling days, the substrates were analyzed for the inorganic species. The 41 samples analyzed represented a variety of chemical and transport regimes. For the analyzed samples, the nitrate and sodium ions were found in the coarse mass fraction (1.0–10.0 μm), while the sulfate and ammonium ions were found, as expected, in the 0.1–1.0 μm, or fine size, range.

[25] The molar concentrations of sulfate, ammonium, nitrate, and sodium are summarized in Table 1. Because the majority of nitrate and sodium mass concentrations were in the coarse mode and the molar ratio of sodium to nitrate was about 1, it will be assumed that nitrate was in the form of $NaNO_3$ and, furthermore, that sulfate was in the form of ammoniated sulfate. The presence of Ca^{2+} in the coarse mode suggests that $Ca(NO_3)_2$ may also be present, although we did not consider this species in our analyses. It is noteworthy to point out that the IMPROVE and URG samplers used for measurements of the fine mode employed a cyclone inlet with a cutpoint aerodynamic diameter of 2.5 μm, which was typically near the middle of the coarse mode nitrate and sodium distributions. Concurrent number size distributions, reported by *Hand et al.* [2002], showed that, in general, the fine and coarse modes of the derived volume size distributions were also separated at about 1.0 μm aerodynamic diameter.

4. Summary of Aerosol Species Concentrations

[26] Fine mass species concentrations, as measured by the IMPROVE or URG (used for ion concentrations) samplers, are summarized in Table 2. Out of 125 sampling days, there were 111 days where species concentrations were recovered from all sample modules. The molar ratio of Na to NO_3 for this larger data set was again near 1 at approximately 1.05, suggesting that nitrate was in the form of sodium nitrate. Sodium nitrate was estimated by multiplying the nitrate ion mass concentration by 1.37. An OLS regression between gravimetric mass and the sum of the aerosol species masses discussed above yielded an $R^2 = 0.90$ and a slope of 1.02 ± 0.02,indicating good closure between these two estimates. Measured gravimetric fine mass (laboratory RH was between 40 and 50%) was about 7% greater than reconstructed fine mass with ammoniated sulfate contributing 51% of the mass and organics and soil contributing 21 and 22%, respectively.

5. Comparison of Equilibrium Models

[27] To represent atmospheric aerosol water contents as functions of RH, two different thermodynamic models were explored for use in this work: AIM [*Clegg et al.*, 1998b] and ISORROPIA [*Nenes et al.*, 1998]. AIM and ISORROPIA can be run in various configurations that predict the equilibrium state of the system, including partitioning of species between the liquid, solid, and gaseous phases. Here we specified the mass concentrations of aerosol-phase species based on the filter measurements described earlier, and used the models only to compute the equilibrium aerosol water contents over a range of RH from 20 to 90%.

[28] The version of AIM used here considers systems composed of sodium-ammonium-chloride-sulfate-nitrate-water at 298.15 K. Equilibrium states are calculated using Gibbs' energy minimization, using a global search to find the minimum. The calculations of activities of water and ions present in the aqueous phase utilize the Pitzer, Simonson, and Clegg equations [*Pitzer and Simonson*, 1986; *Clegg et al.*, 1992]. The model considers 19 possible solid phases and is valid for concentrations to saturation with respect to the solid phases. Thus it is not generally applicable to supersaturated, metastable solutions, although the user is permitted to run in this mode, which suppresses precipitation of solids. We checked the metastable water contents against the predictions of an alternative version of

Table 2. Statistical Summary of Fine Mass Species Concentrations[a]

Fine Mass Concentrations				
Variable, μg m^{-3}	Mean	Standard Deviation	Minimum	Maximum
Fine mass (FM)	6.87	4.26	0.21	19.22
Reconstructed FM	6.39	3.68	1.02	17.09
Ammonium ion	0.68	0.43	0.11	2.04
Sulfate ion	2.52	1.83	0.30	8.57
Ammoniated SO_4	3.27(0.51)	2.46	0.22	11.30
Nitrate ion	0.16	0.87	0.02	0.45
Sodium ion	0.063	0.04	0.002	0.23
$NaNO_3$	0.21(0.03)	0.14	0.02	0.87
OCM	1.33(0.21)	0.78	0.13	5.10
LAC	0.15(0.02)	0.10	0.00	0.52
SOIL	1.43(0.22)	1.74	0.03	8.63

[a]The parenthetical values are the fraction that each respective species contributes to reconstructed fine mass. The number of samples is equal to 111.

Table 3. Index of Refraction and Densities Used in Mie Theory Calculations

Variable	Density, g cm^{-3}	Index of Refraction
Ammoniated sulfate	1.78	varies between 1.41 and 1.52 depending on ammoniation
$NaNO_3$	2.26	1.59

AIM [*Clegg et al.*, 1998a] that is more applicable to those cases, and found the differences in aerosol water content leading to negligible differences in predicted ratios of wet to dry scattering (f(RH)) for the species considered in this paper. The composition dependence of the deliquescence RH is included in the formulations while the efflorescence behavior is not.

[29] ISORROPIA considers the same chemical components as AIM, but only allows nine possible solid phases. The solution scheme differs from that used in AIM in that 15 equilibrium reactions are solved, using a fast and stable solution algorithm [*Nenes et al.*, 1998] and permitting only certain aerosol and solution compositions depending on the ratios and $R_{Na} = [Na^+]/[SO_4^{2-}]$ and $R_{SO_4} = \{[Na^+] + [NH_4^+]\}/[SO_4^{2-}]$. These ratios are used to define combinations of sulfate-rich, sulfate-poor, sodium-rich, and sodium-poor domains, along with the appropriate subsets of possible solid and ionic species. This method is called ''divided composition domain'' [e.g., *Ansari and Pandis*, 1999]. Binary activity coefficients are calculated using the Kusik and Meissner relationships, whereas multicomponent activity coefficients are obtained from Bromley's formula. The water content of aerosols is computed from the Zdanovskii-Stokes-Robinson (ZSR) relationship.

[30] ISORROPIA differs from earlier equation-based models in that the mutual deliquescence relative humidity (MDRH) of mixtures of salts is considered. The value of the MDRH depends upon the mixture composition, but is always less than the minimum deliquescence humidity of any of the individual salts, so that the presence of an aqueous phase may be predicted by ISORROPIA where simpler models would predict a dry aerosol. It is important to note, however, that ISORROPIA uses data from the phase diagrams of *Potukuchi and Wexler* [1995a, 1995b] to determine the deliquescence relative humidity (DRH); since not all possible compositions are represented, DRH behavior must be approximated from other combinations of species in such cases. The water contents in the MDRH regions are obtained by assuming a RH-weighted mean between the completely dissolved state for the most hygroscopic salt, and the completely dry state of the aerosol. This contrasts with the treatment in AIM, which solves the full minimization problem and thus can predict the gradual dissolution of solids.

[31] ISORROPIA can also be used to compute water contents for the metastable phase. In this mode the formation of solid phases is suppressed, and calculations are made for the aqueous phase assuming the applicability of the necessary thermodynamic data at RHs below deliquescence. Since solid formation is not allowed for the metastable calculations, crystallization cannot be explicitly modeled. Instead, efflorescence behavior is approximated by assuming the applicability of crystallization points for ammoniated sulfate salts that are reported in the literature. Then, for calculations below these crystallization RHs, the thermodynamic data are not further extrapolated but instead a fixed, highly concentrated solution composition is assumed, leading to a discontinuity in predicted water contents that approximates the crystallization behavior.

[32] The models were used to estimate D/D_o growth and f(RH) curves for each sampling period. For purposes of comparing these models, log normal aerosol mass size distributions were assumed for both the fine and coarse modes with geometric mass mean diameters of 0.38 and 3.0 μm, respectively, and a geometric standard deviation of 1.9 for both modes. These size parameters were derived from the average for the 41 MOUDI samples, as discussed further in the next section. Densities and indices of refraction for aerosol mixtures were based on 24-hour composition data and used the inputs listed in Table 3.

[33] f(RH) curves were calculated for ammoniated sulfate assuming all sulfate occurred in the fine mode, while sodium nitrate was assumed to be in the coarse mode with size parameters discussed earlier. Because the nephelometers and fine particle samplers were operated with 2.5 μm cutpoints, the average mass size distribution for sodium nitrate (coarse mode) was multiplied by the sampler efficiency curve in an effort to estimate the f(RH) curves only for the fine component of the coarse mode.

[34] Mean, maximum, and minimum differences between the metastable models are listed in Table 4. In about one-third of the cases, the metastable AIM f(RH) curve is well below (more than a few percent) that of ISORROPIA above the crystallization point, implying that the AIM model predicts less aerosol water than ISORROPIA. Below the crystallization point as estimated by ISORROPIA, the AIM model predicts some dissolved water and smoothly approaches zero as RH approaches zero. For a few cases the reverse was true. In general, for the metastable models, the maximum difference is always near the crystallization point with differences approaching zero for high RH values.

[35] Generally, the deliquescence points predicted by the two models were the same within a few RH percent-

Table 4. Statistical Summary of the Mean Percent Difference Between f(RH) Curves in Specific Relative Humidity Ranges That Were Derived From Aerosol Growth Predicted by the AIM and ISORROPIA Models[a]

	ISORROPIA Minus AIM (Metastable)		
RH	Mean	Minimum	Maximum
15–20	−0.06	−0.13	0.03
20–25	−0.10	−0.17	0.01
25–30	−0.14	−0.21	−0.01
30–35	−0.17	−0.25	−0.03
35–40	−0.01	−0.06	0.08
40–45	−0.01	−0.06	0.08
45–50	0.00	−0.06	0.07
50–55	0.00	−0.05	0.07
55–60	0.00	−0.04	0.06
60–65	0.01	−0.03	0.05
65–70	0.01	−0.04	0.05
70–75	0.02	−0.04	0.05
75–80	0.02	−0.03	0.05
80–85	0.03	−0.02	0.06
85–90	0.03	−0.01	0.07
90–95	0.00	−0.04	0.06

[a]The number of data points is 66.

Table 5. Statistical Summary of Integrating Nephelometer Measurements (JD = 237 – 302)[a]

Variable, Mm^{-1}	Mean	Standard Deviation	Minimum	Maximum
b_{open}	24.16	16.20	6.66	63.54
b_{10}	25.11	17.25	6.13	65.71
$b_{sp2.5wet}$	21.88	15.91	4.49	61.87
$b_{sp2.5dry}$	17.74	13.47	2.91	53.76
$b_{op} - b_{sp2.5wet}$	2.29	1.22	0.65	8.07
$b_{sp2.5wet} - b_{sp2.5dry}$	4.14	3.46	0.58	17.87

[a]The number of data points was 54.

age points and, because the AIM model accounted for intermolecular interactions, the AIM model predicted deliquescence points which were less ''abrupt'' than ISORROPIA. Therefore as with the metastable branch, the maximum difference between the models occurred at the deliquescence points.

6. Comparison Between Measured and Modeled Dry Scattering Coefficients

[36] Table 5 summarizes the integrating nephelometer measurements for the time period common to all instruments. While most nephelometer measurements were initiated on Julian Day 180, the dry integrating nephelometer and humidograph measurements did not start until Julian Day 237 and continued to Julian Day 302. The 2-min data were averaged up to 24 hours and only those days with at least 450 data points (15 hours) were included in the table. Comparison of the open air and PM_{10} nephelometers showed that they compared to within 4%, implying that, on the average, there was little or no contribution to scattering by particles larger than 10 μm. The average difference between the open air and $PM_{2.5}$ nephelometers was 2.29 Mm^{-1}, or 9%. Because the open-air nephelometer may underestimate coarse particle scattering by as much a factor of 2 [*Molenar*, 1997], the contribution of coarse particles to scattering may be as great as 17–18%. The average difference between ambient and dry scattering below 2.5 μm was 4.14 Mm^{-1}, or 19%, but episodically was as high as about 30%.

[37] Because little difference, on the order of 10% or less [*Ouimette and Flagan*, 1982; *Sloane*, 1986; *Malm and Kreidenweis*, 1997; *Malm et al.*, 2000b] has been found between scattering predicted by internally and externally mixed aerosol models, the following externally mixed model was used to estimate reconstructed particle scattering:

$$b_{scat} = (e_{sf})f_s(RH)[\text{Ammoniated } SO_4] + (e_{nf})f_n(RH)[NaNO_3] + (e_{omcf})f_{omc}(RH)[OMC] + (e_{soilf})[SOIL]. \quad (1)$$

[38] The brackets indicate the species concentration, while e_{sf}, e_{nf}, e_{omcf}, and e_{soilf} refer to the fine or $PM_{2.5}$ dry mass scattering efficiencies of ammoniated sulfate, sodium nitrate, organic carbon, and soil mass concentrations, respectively, and the f(RH) term is the scattering enhancement term associated with particle growth as a function of RH as obtained from the thermodynamic and Mie scattering models.

[39] Average dry mass scattering efficiencies, e_{sf}, geometric mass mean diameters, d_g, and standard deviations, σ_g, of ammoniated sulfate were calculated using MOUDI data, corrected to physical diameter. These calculations are summarized in Table 6 and Figure 1. Figure 1 shows the relationship between these variables for the 41 MOUDI sample days. Some interesting relationships are readily apparent. As might be expected, as σ_g increased e_{sf} decreased (Figure 1a). More interesting, at low mass levels (<2 μg m^{-3}) σ_g varied between about 1.4 and 2.5; however, at higher mass levels the variability in σ_g decreased (mass size distribution narrowed) and approached 1.4 at the highest-mass loadings (Figure 1b). This narrowing of σ_g as mass levels increase was reflected in the relationship between mass and mass scattering efficiencies. Generally, as mass increased so did mass scattering efficiency (Figure 1c). Also, distributions with large mass mean diameters (>0.44 μm) had mass scattering efficiencies that varied from 2.5 to 4.0 m^2 g^{-1} and σ_g that varied between 1.4 and 2.5, while those size distributions with mass mean diameters less than about 0.28 μm had efficiencies of about 2.5 m^2 g^{-1} and σ_g of about 1.6 (Figures 1d and 1e). Furthermore, Figure 1f shows that at low mass loadings the mass mean diameter varies from 0.24 to 0.48 μm, while at higher mass loadings d_g varies less. These relationships were similar to those found by *Hand et al.* [2002] using measured number size distributions; however, those authors assumed that all aerosol species were internally mixed.

[40] Because mass size distribution data were only available on 41 out of 104 sampling periods, an effort was made to capture the general relationships presented in Figure 1 and apply them to the full data set. To account for the daily variations in the mass scattering efficiency for ammoniated sulfate, e_{sf} was varied as a function of ammoniated sulfate mass using 2.4 + 0.42* (ammoniated sulfate) below ammoniated sulfate mass equal to 2.0 μg m^{-3} and 3.2 + 0.07* (ammoniated sulfate) above 2.0 μg m^{-3}. Mass scattering efficiencies assumed for organics and soil were 4.0 and 1.0 m^2 g^{-1}, respectively [*Trijonis et al.*, 1990; *Malm et al.*, 1994], while that used for sodium nitrate was 1.6 m^2 g^{-1}. The average of the 41 MOUDI samples is 1.6 m^2 g^{-1}, assuming that nitrate was in the form of sodium nitrate with its peak in the coarse fraction. The efficiency of the IMPROVE 2.5 μm cyclone inlet was used to apportion only the nitrate in particles smaller than 2.5 μm to $PM_{2.5}$ scattering.

[41] Table 7 contains a summary of measured and reconstructed dry scattering coefficients along with the scattering

Table 6. Statistical Summary of Size and Scattering Properties of $PM_{2.5}$ Ammoniated Sulfate Mass[a]

Variable	Mean	Standard Deviation	Minimum	Maximum
Ammoniated sulfate mass, μg m^{-3}	3.65	3.31	0.50	12.04
d_g, μm	0.38	0.05	0.26	0.47
σ_g	1.88	0.26	1.50	2.42
eff_d, m^2 g^{-1}	3.15	0.43	2.42	4.06

[a]The number of data points was 41.

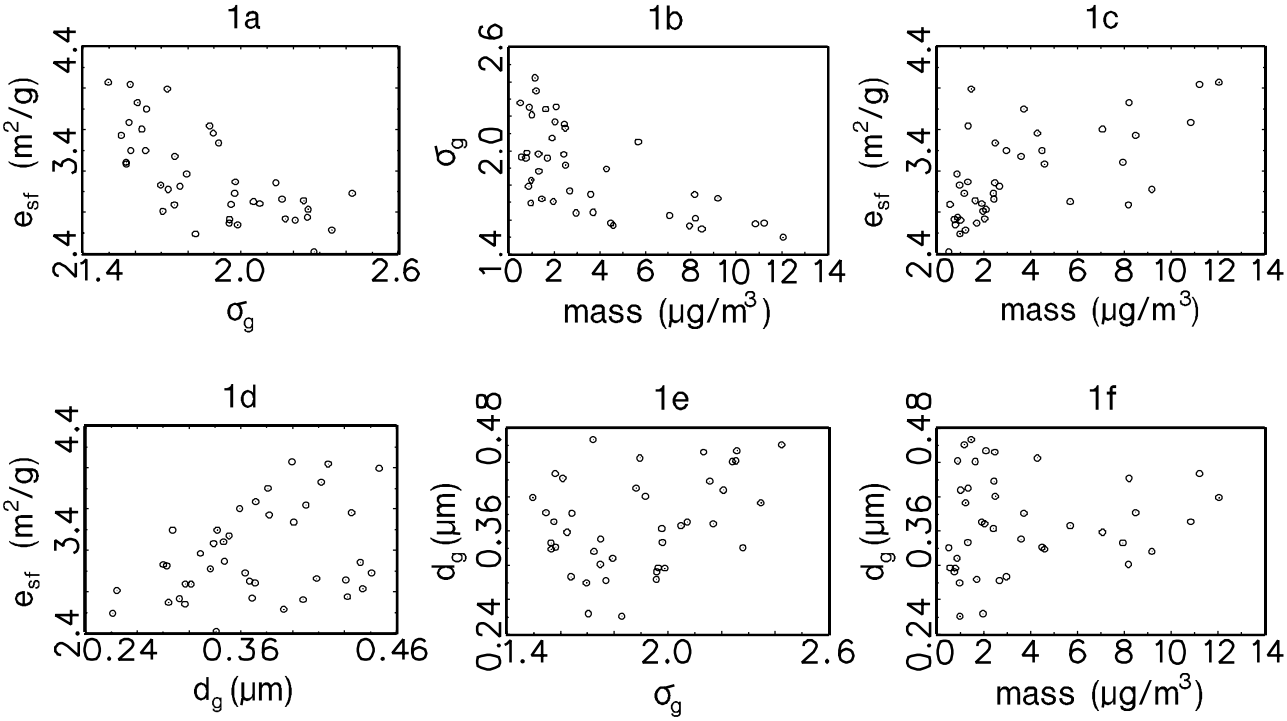

Figure 1. (a–f) Multiple scatterplots of ammoniated sulfate dry mass scattering efficiency (eff_d), geometric mass mean diameter (d_g), geometric standard deviation (σ_g), and ammoniated sulfate mass for the 41 days on which MOUDI size mass size distribution were made.

coefficient contribution associated with each species. The difference between average measured and reconstructed dry scattering was 4%. The parenthetical values represent the fraction of scattering associated with each species. A linear regression of measured scattering as the dependent variable and reconstructed scattering as the independent variable yielded $R^2 = 0.93$ an with a slope of 0.96 ± 0.03 and an intercept term of 0.11 ± 0.62. Thus we conclude that the model as given by equation (1) reproduced measured dry scattering quite well.

7. Comparison of Measured and Modeled Ambient (Wet) Scattering Coefficients

[42] Table 8 summarizes the comparisons of measured and modeled ambient scattering coefficients as well as the contribution of each species to ambient scattering coefficients based on equation (1). Twenty-four hour average deliquescence and crystallization *f*(RH) values were calculated for ammoniated sulfate and sodium nitrate for each of the three equilibrium models described earlier by averaging hourly *f*(RH) values. As discussed previously, it was assumed that all sulfate and ammonium were in the fine mode while nitrate was in the form of sodium nitrate and had a concentration peak in the coarse mode. The *f*(RH) of sodium nitrate was based on the fraction of this $NaNO_3$ mass in particles smaller than 2.5 μm. It was assumed that the aerosol composition and size distribution were constant over a 24-hour period, but the water contents varied hourly as a function of RH. *f*(RH) for organics was assumed to be 1, that is, they were assumed to be nonhygroscopic.

[43] As pointed out above, ISORROPIA predicted almost no water below the crystallization point for the metastable branch, while under the "no solids" option the AIM model predicted some water below this point. Some examples of the effect that, assuming water contents as given by either the crystallization or deliquescence branch, had on predicted scattering are presented in Table 8. Average modeled dry scattering was 16.01 Mm^{-1} while average ambient scattering using the AIM metastable *f*(RH) curve and hourly values of RH was 20.80 Mm^{-1}, which is nearly equal (1% difference) to the average measured ambient scattering value of 20.94 Mm^{-1}. Even though the AIM metastable branch ascribed some water to the aerosol below the ISORROPIA crystallization point, the average ambient scattering predicted using the ISORROPIA model was only about 1.5% less than the model using the AIM metastable solution assumptions. Using the AIM deliquescence branch yielded an ambient-modeled

Table 7. Statistical Summary of Reconstructed and Measured Dry Fine Mass Scattering and the Scattering Associated With Each Species Assuming a Model Represented by Equation (1)[a]

Scattering, Mm^{-1}	Mean	Standard Deviation	Minimum	Maximum
Reconstructed	18.45	12.49	3.56	63.17
Measured	17.73	13.30	2.27	53.76
Sulfate	12.31(0.67)	9.77	1.07	42.08
Nitrate	0.26(0.01)	0.12	0.11	0.84
Organics	5.11(0.28)	3.35	0.52	20.41
Soil	0.77(0.04)	0.96	0.06	3.73

[a]The parenthetical values are the fraction of scattering associated with each species. The number of data points was 64.

Table 8. Statistical Summary of Measured and Reconstructed Ambient Fine Mass Scattering and Scattering Associated With Each Species[a]

Variable	Mean	Standard Deviation	Minimum	Maximum
RH, %	44.63	11.68	20.92	74.38
Measured ambient $b_{sp.25}$, Mm^{-1}	20.94	13.71	3.62	61.87
SOIL, Mm^{-1}	1.43(6.9)	1.78	0.06	8.63
OCM, Mm^{-1}	5.13(24.7)	3.74	0.60	26.67
Sulfate ambient (AIM metastable), Mm^{-1}	13.64(65.6)	10.89	1.77	52.16
Sulfate dry, Mm^{-1}	9.11	7.49	1.02	40.13
Nitrate ambient (AIM metastable), Mm^{-1}	0.60(2.9)	0.38	0.14	1.99
Nitrate dry, Mm^{-1}	0.34	0.19	0.11	0.99
Theoretical dry $b_{sp2.5}$, Mm^{-1}	16.01	10.66	3.24	67.47
Theoretical ambient $b_{sp2.5}$ (AIM metastable), Mm^{-1}	20.80	13.74	4.71	79.61
Theoretical ambient $b_{sp2.5}$ (AIM deliquescence), Mm^{-1}	18.33	12.58	3.68	74.05
Theoretical ambient $b_{sp2.5}$ (ISO metastable), Mm^{-1}	20.49	13.92	4.33	81.00

[a]Ambient scattering predictions resulting from using different equilibrium model assumptions are also presented. The parenthetical values are the percent scattering associated with that species assuming the AIM metastable equilibrium model. The number of data points was 104.

value of 18.33 Mm^{-1} which was about 12% less than the average theoretical value using AIM metastable branch.

[44] Based on this analysis, the model using metastable water content from AIM to compute the f(RH) curves yielded the best overall fit to measured ambient scattering. An OLS estimate, with measured and theoretical ambient scattering and with the AIM metastable f(RH) curves as the dependent and independent variables, respectively, resulted in an R^2 of 0.90 with a slope of Using the ISORROPIA metastable f(RH) curves only marginally degraded the comparison between modeled and measured ambient scattering, while use of the deliquescence f(RH) curves significantly degraded the fit (>10%), implying that, in general, the ambient aerosols had been exposed to RHs greater than the deliquescence RH and were on the crystallization branch of the curve. Despite the good agreement between predictions and measurements that was found with this approach, it is also possible that other species, namely organic carbon compounds, were responsible for the retention of water that we attribute to the metastable water associated with inorganic compounds. We explore this possibility further in the following sections.

[45] Assuming the AIM metastable state water content and the external mixture model, sulfates and organics contributed 65.6 and 24.7% of $PM_{2.5}$ ambient scattering while soil contributed 6.9% and nitrates contributed 2.9%. The difference between theoretical ambient and dry $PM_{2.5}$ scattering was about 4.8 Mm^{-1} or 19%, implying that despite the study-average RH of only 44%, 19% of ambient scattering was associated with sulfate and nitrate water absorption. Ambient sulfate scattering was 33% greater than dry scattering while $PM_{2.5}$ nitrate scattering, which was small compared to sulfate scattering, increased by 43%. Also, 19% was close to the scattering difference measured by the ambient and dry $PM_{2.5}$ nephelometers. It should be noted that the calculations presented in Table 8 are for 104 sampling days while concurrent ambient and dry nephelometer scattering data were available on only 54 days.

[46] The "best fit" model assumed only inorganic salts were hygroscopic and that their hygroscopicity was described by the AIM metastable f(RH) curve. These assumptions can be further explored by comparing measured f(RH) curves to those theoretically estimated using the model described by equation (1) in combination with f(RH) curves associated with various equilibrium models and the assumption concerning the hygroscopicity of carbonaceous material.

8. Comparison of Measured and Theoretical Scattering Coefficients as Functions of Relative Humidity

[47] To estimate f(RH) curves, one Radiance Research nephelometer was operated continuously in a dry mode while a second nephelometer was scanned through RHs that ranged from about 20 to 90%. The ambient aerosol was first dried from ambient RH, usually about 40%, to RHs less than ambient and then humidified to humidities greater than ambient. Figure 2 shows a typical RH "scan" (Julian Day 284) with the dotted and solid lines representing the dry and RH-dependent nephelometers, respectively, and the inset showing the resultant f(RH) curve. The minute-to-minute changes in aerosol concentration as represented by the dry scattering were quite variable. In this example, during the first half of the day aerosol scattering was approximately 10 Mm^{-1}, while during the second half aerosol scattering was more variable and on the average about 30 Mm^{-1}. During the scan the dry scattering varied between 20 and 30 Mm^{-1}. The ambient f(RH) curves were then calculated by dividing the instantaneous variable-RH b_{scat} by the instantaneous dry scattering coefficient, $b_{scat}(RH)/b_{scat}(RH_{min})$. Not accounting for the short term, temporal variability of dry scattering would introduce significant error into the f(RH) determination.

[48] Operating the humidograph in this configuration could have resulted in: (1) observation of crystallization if the ambient aerosol had been exposed to RHs above its deliquescence point and the crystallization point was below the ambient RH, (2) observation of deliquescence if the aerosol had not been exposed to humidities above the deliquescence point and the ambient RH was below the deliquescence point, or (3) observation of a continuous f(RH) curve over the entire RH range.

[49] Because aerosol speciation data were collected using filter measurements that aggregated aerosol concentration into 24-hour averages, direct comparison of 24-hour theoretical f(RH) curves based on the use of equation (1) to measurements of f(RH) that were made on the timescale of a

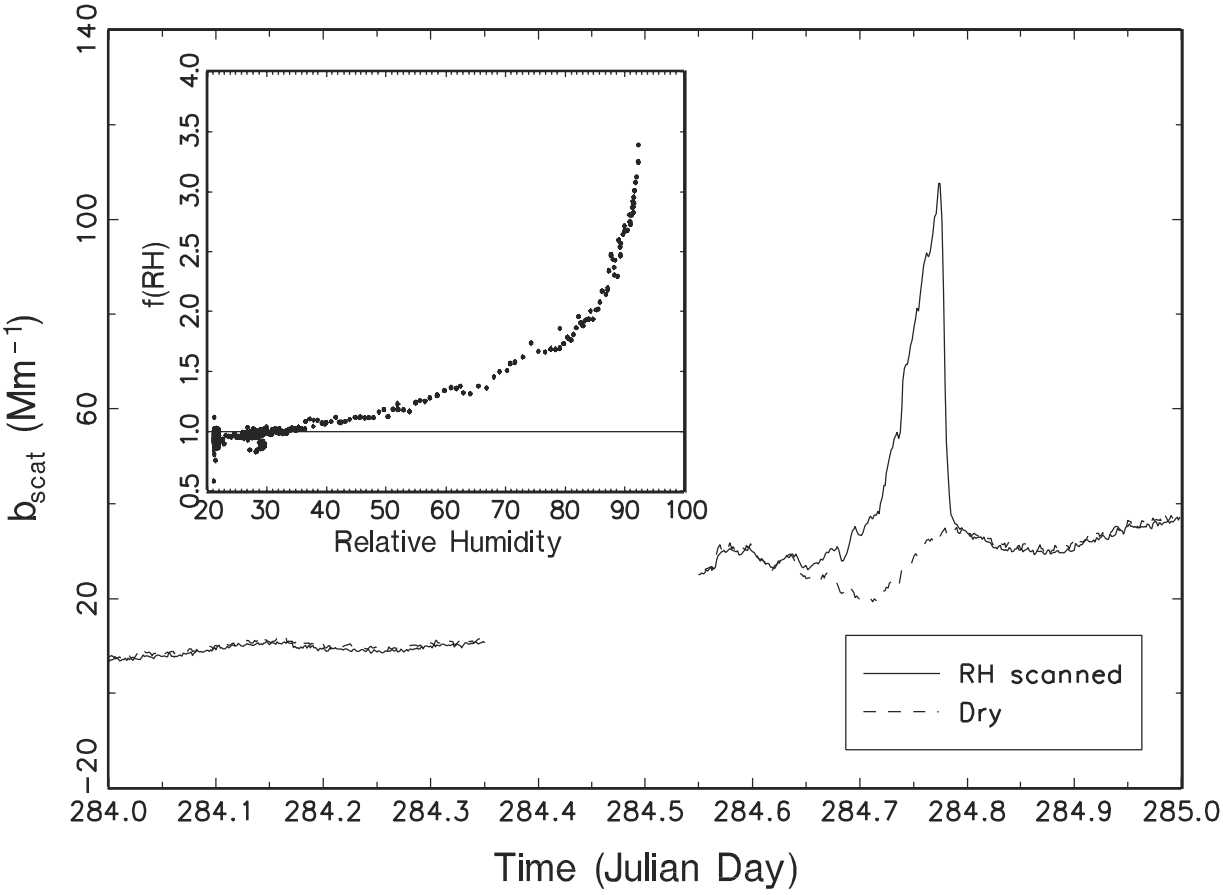

Figure 2. An example of dry and relative humidity ramped scattering coefficient for Julian Day 284. The hours showing missing data correspond to a calibration period.

few hours was problematic. *Hand et al.* [2002] reported dry scattering estimates derived from dry number size distribution measurements which show that fine particle scattering and aerosol concentration track each other (R^2 = 0.97) on timescales on the order of minutes, suggesting that sulfate and organic mass concentrations, the primary constituents of the fine mode, varied temporally in proportion to dry scattering. Furthermore, *Hand et al.* [2002] reported a high degree of correlation between dry scattering and highly time-resolved sulfate measurements. An OLS regression between the two variables resulted in an R^2 = 0.86. Therefore, to account for the small-timescale variation (<1 hour), the 24-hour average sulfate and organic mass concentrations were temporally scaled to the dry nephelometer data such that the sulfate and organic scaled data integrated to the 24-hour average concentrations but reflected short-timescale fluctuations.

[50] The dry and RH scanned $PM_{2.5}$ nephelometer measurements were simulated using equation (1) with f(RH) = 1 for organics and with the temporally adjusted sulfate and organic data on a two-minute-by-two-minute basis. Soil and nitrate mass concentrations were not adjusted for short term temporal fluctuations, and the mass scattering efficiencies applied for these species were those determined for that fraction of their masses found in the fine aerosol mode. Theoretical ambient f(RH) curves were then calculated using $b_{scat}(RH)/b_{scat}(RH_{min})$.

[51] Forty-four f(RH) scans were made between Julian Days 238 and 301. The average measured and calculated f(RH) values are summarized in Table 9. Figures 3, 4, 5, and 6 show four general types of behavior of ambient and theoretical f(RH) curves. The solid line in each figure is a running three-point average of 2-min data while error bars are plotted for every fifth data point. The uncertainty associated with RH is calculated from the uncertainty inherent in the RH sensor (±2%) [*Rotronic Instrument Corp.*, 1998] and from the uncertainty in RH caused by a change in temperature inside the nephelometer. The exact RH inside the nephelometer is unknown; however, it is bounded by the RH at the inlet and outlet of the instrument. At low RH, this difference is less than 1% (as estimated from a temperature difference of 0.3°C), while at 90% RH the difference in RH is on the order of 2%. Therefore the combined uncertainty is on the order of ±3% at high-RH values and less at lower humidities. To be conservative, the maximum uncertainty of ±3% is presented in Figures 3–6. The uncertainty in f(RH) is based on a nephelometer measurement uncertainty of 5% [*Molenar*, 1997].

[52] The dotted and dashed lines correspond to various model calculations. There were 5 days where there was a clear deliquescence point; one day, Julian Day 275, is shown in Figure 3. The model calculations shown in Figure 3 were based on the AIM ammoniated sulfate deliquescence growth for an ammonium to sulfate ratio of 1.74. There

Table 9. Statistical Summary of Measured *f*(RH) in 5% Relative Humidity Increments

RH	Mean	Standard Deviation	Minimum	Maximum	*N*
20–25	0.93	0.20	−1.53	4.52	2526
25–30	0.99	0.11	−1.80	1.82	4824
30–35	1.02	0.13	−2.01	8.39	5984
35–40	1.07	0.07	0.83	1.38	997
40–45	1.11	0.07	0.92	1.43	209
45–50	1.15	0.08	0.91	1.45	202
50–55	1.21	0.07	1.00	1.40	261
55–60	1.28	0.09	1.00	1.57	169
60–65	1.38	0.12	1.03	1.67	159
65–70	1.48	0.16	1.04	1.90	170
70–75	1.67	0.19	1.13	2.09	175
75–80	1.76	0.14	1.30	2.34	440
80–85	2.06	0.25	1.55	3.07	390
85–90	2.64	0.43	1.80	4.49	442
> 90	3.18	0.47	1.97	5.05	456

were two modeled deliquescence points at about 68 and 75%, which correspond closely to the measured deliquescence points. On Julian Day 301 the ammonium to sulfate molar ratio was 1.8, and again the modeled and measured deliquescence points match were within a few RH percentage points. However, on three other days when the ammonium to sulfate ratio was measured to be near 2 (fully neutralized), the model-predicted deliquescence points, as expected, were near 80% while the measured deliquescence points were at approximately 65–70% RH. Undoubtedly, the hygroscopic salt was not pure ammonium sulfate. On one of the 3 days MOUDI mass size distribution data were available and did show 1.1 and 0.22 nmol m^{-3} of K^+ and Ca^{2+} in addition to 43.0 nmol m^{-3} of NH_4^+ and 22.2 nmol m^{-3} of SO_4^{2-}. However, neither the ISORROPIA nor AIM models incorporate K^+ or Ca^{2+} in the equilibrium calculation. The average mean difference relative to the measured *f*(RH) curve above 80% was 17%.

[53] Figure 4 shows 1 of 5 days, Julian Day 286, where there are intimations of observed crystallization. Also, shown in Figure 4 is the modeled *f*(RH) curve based on the ISORROPIA metastable water absorption curve. There was close agreement between the predicted and measured *f*(RH) curves, and the measured and modeled crystallization points agreed well. The ISORROPIA model was used because it predicts a crystallization point, whereas the AIM model, exercised in the metastable configuration, does not. On all 5 days the measured and predicted crystallization points agreed to within a few RH percentage points and the *f*(RH) curves agreed well above the crystallization points. The average difference for the 5 days between measured and theoretical *f*(RH) curves above 35% RH was less than 1%.

[54] Figure 5, measured on Julian Day 238, represents a third type of *f*(RH) curve of which there are also five cases.

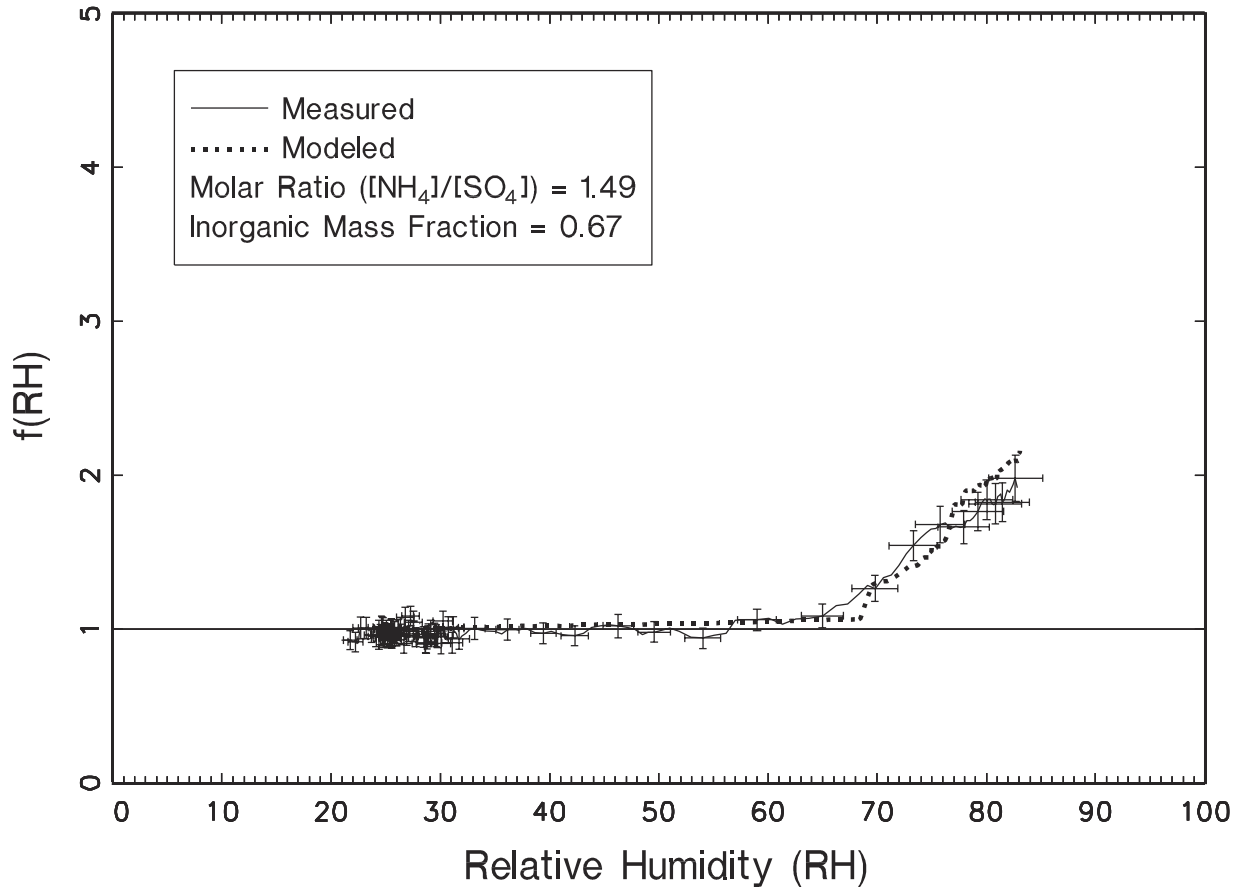

Figure 3. An example of measured and modeled *f*(RH) curves where deliquescence was observed for Julian Day 275. The molar ratio of ammonium to sulfate was 1.49 and the inorganic (SO_4 + NH_4 + NO_3 + Na) fine mass fraction was 0.67.

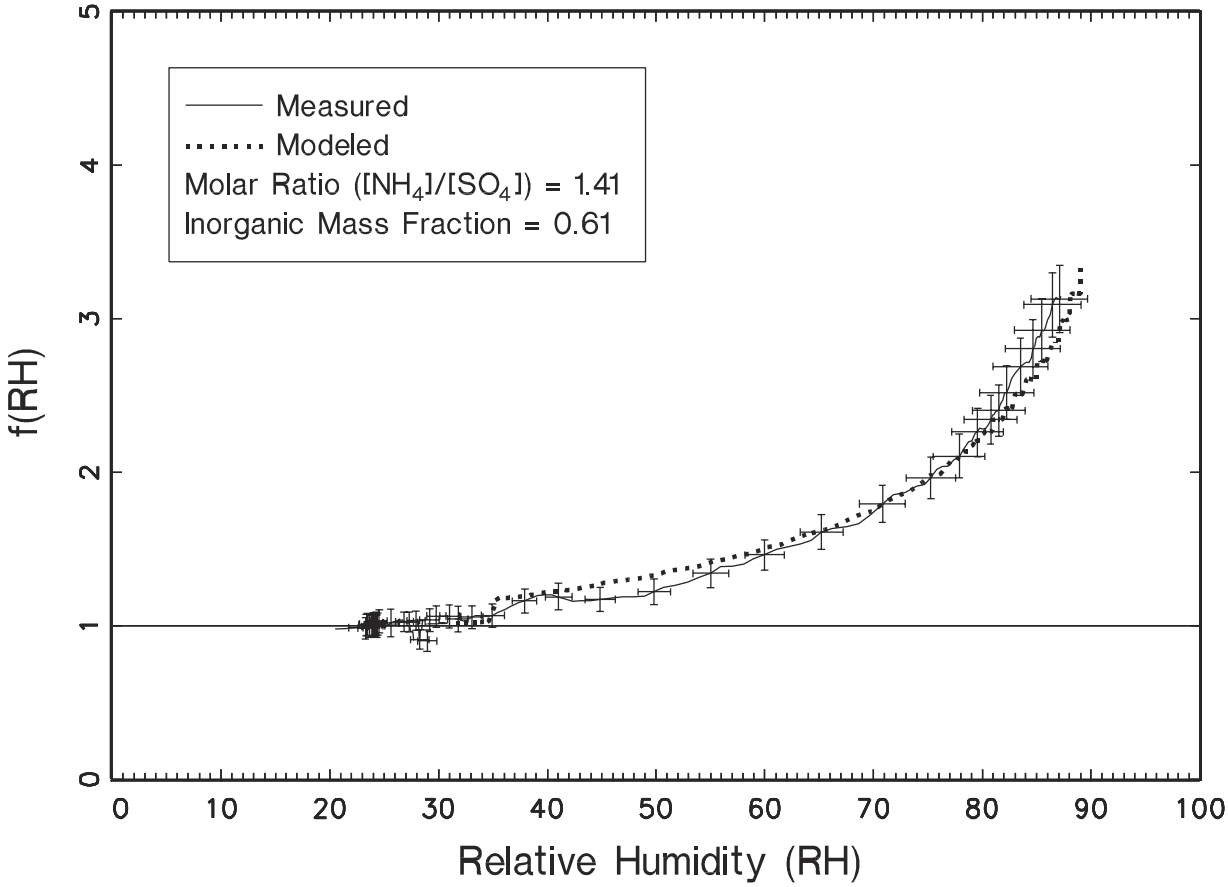

Figure 4. An example of measured and modeled *f*(RH) curves for a day where crystallization was observed. The molar ratio of ammonium to sulfate was 1.41 and the inorganic (SO_4 + NH_4 + NO_3 + Na) fine mass fraction was 0.61.

The measured and calculated *f*(RH) curves agreed well above the deliquescence point; however, below the deliquescence point the measured curve did not fall on either the ascending or descending branch of the growth curve but varied smoothly between the two points, and exhibited neither deliquescence nor crystallization. On all 5 days water uptake began at RHs of about 30–35%. Above 80% RH the average difference between observed and modeled *f*(RH) for all 5 days was again about 1%.

[55] Figure 6, measured on Julian Day 242, shows an example of the predominant type of *f*(RH) pattern of which there were 29. The 29 measured *f*(RH) curves again were continuous, indicating no crystallization or deliquescence from approximately 1 to their respective maximum values. The two theoretical *f*(RH) curves in Figure 6 are based on AIM and ISORROPIA-derived metastable growth curves. The RH scan for the measured *f*(RH) curve was initiated at a RH between 26 and 28%, which was below the crystallization point predicted by ISORROPIA. Therefore the dry scattering coefficient based on the ISORROPIA model at 26% RH did not have any contribution due to water, while the dry scattering estimate based on AIM did. Therefore when estimating *f*(RH) using $b_{scat}(RH)/b_{scat}(RH = 26\%)$, the AIM based *f*(RH) curve was a significant fraction lower than the ISORROPIA based *f*(RH) curve because the AIM based $b_{scat}(RH = 26\%)$ was larger than ISORROPIA. The measured and AIM based *f*(RH) curves were in better agreement than assuming a "dry" aerosol at 26–28%, suggesting that the aerosol was not "dried out" at the beginning of the RH ramp.

[56] Table 10 summarizes percent differences between measured and modeled *f*(RH) for the 29 days in increments of 5% RH. The mean difference varied from a low of −1.6 to 4.9% at 85–90% RH range. The average difference above 35% RH between measured and predicted *f*(RH) curves over all 29 days was on the order of 1%. The highest organic mass concentrations of 3.8(0.34), 5.1(0.30), and 3.2(0.27) $\mu g\ m^{-3}$ occurred on Julian Days 243, 244, and 245, respectively. The parenthetical values are the fraction of fine mass attributed to organics. The average difference, with *f*(RH) = 1 for carbonaceous material and soil, between measured and modeled *f*(RH) over RH ranges from 35 to 95% on those 3 days was 1.5%.

[57] There were 4 days where the measured *f*(RH) curves were 50–60% greater than the theoretical curves at 90% RH. The average difference above 80% RH for the 4 days was 59%. Two of those days exhibited crystallization in the 35% RH range which was also predicted by the ISORROPIA model, one day showed clear deliquescence at 55% while the model predicted 65%, and one day exhibited continuous growth. All of these days were among those days with the lowest-aerosol concentrations. Organics and

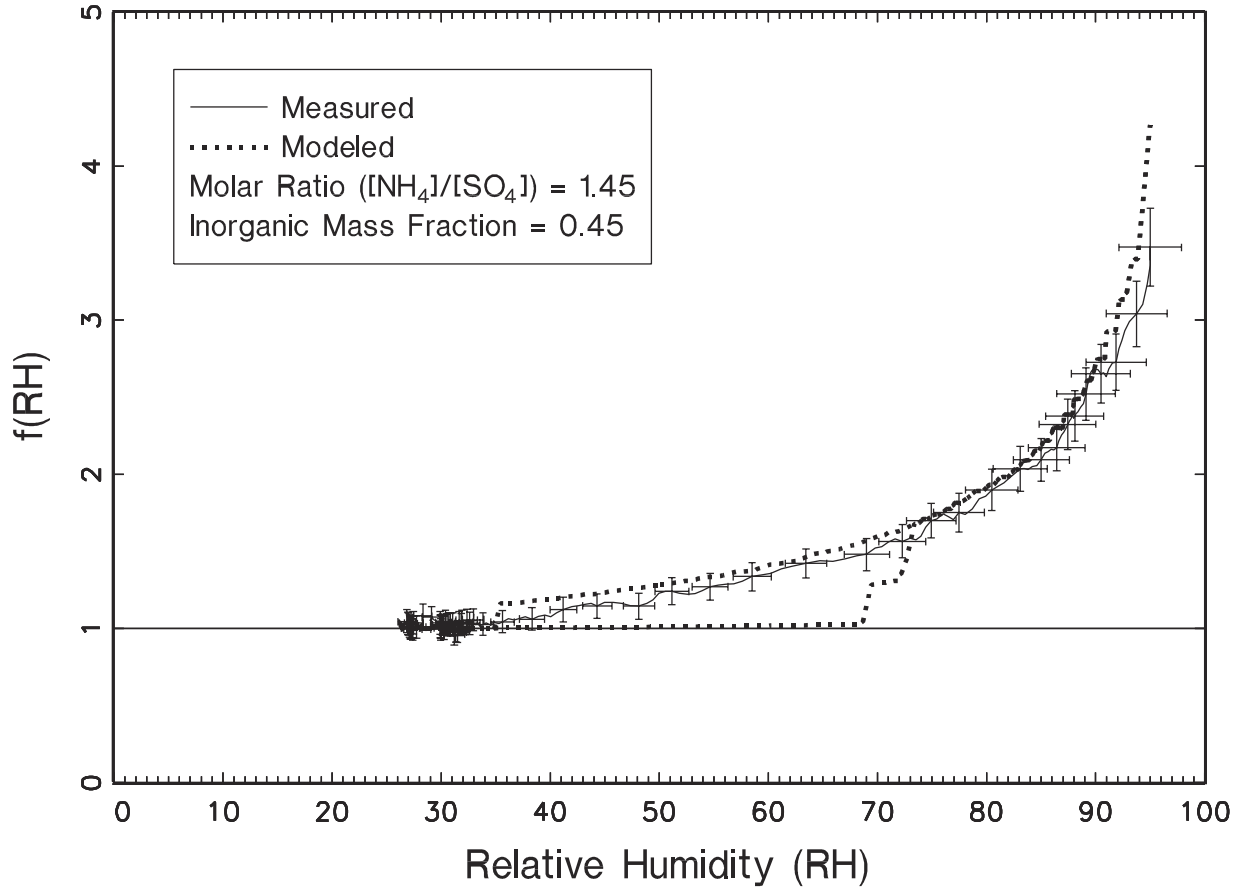

Figure 5. An example of a measured f(RH) curve where neither deliquescence nor crystallization was observed. The modeled f(RH) curve for both deliquescence and crystallization are shown for reference. The molar ratio of ammonium to sulfate was 1.45 and the inorganic (SO_4 + NH_4 + NO_3 + Na) fine mass fraction was 0.45.

ammoniated sulfate were less than about 1 μg m^{-3} which corresponds to a dry scattering coefficient of only about 5–8 Mm^{-1}. Therefore the measured f(RH) curve reflected increased measurement uncertainty. Also, at these low concentrations, the positive organic carbon artifact was on the order of the ambient organic concentration, which can result in a positive or negative bias of reported organic concentrations, depending on whether the blank correction is too large or too small. Overestimation of organic aerosol (underestimation of organic blank correction) would serve to suppress the theoretical f(RH) curve. Another possibility is that on those 4 days organics absorbed about as much water as the inorganic species.

9. Statistical Estimates of Species Specific f(RH) Curves

[58] The amount of scattering at a specific RH associated with individual species can be estimated statistically using:

$$b_{\mathrm{scat,water}}(\mathrm{RH}) = a_0 + a_1[\text{Ammoniated } SO_4] + a_2[\mathrm{OMC}] + \ldots + a_n[\text{Other species}], \quad (2)$$

where $b_{\mathrm{scat,water}}$(RH) is scattering due to water at some RH, $a_1 = e_s\,[f(\mathrm{RH})_s - 1]$, $a_2 = e_{\mathrm{oc}}\,[f(\mathrm{RH})_{\mathrm{oc}} - 1]$ and so forth. a_0 is interpreted as scattering associated with residual water or it can be set to zero, implying that all water scattering is associated with the aerosol species explicitly included in the equation. e_s and e_{oc} are the average dry mass scattering coefficients associated with sulfates and organics, respectively. $b_{\mathrm{scat,water}}(\mathrm{RH}) = b_{\mathrm{scat}}(\mathrm{RH}) - b_{\mathrm{scat,dry}}$ is calculated on a 24-hour sampling-period-by-sampling-period basis by estimating b_{scat}(RH) using measured $b_{\mathrm{scat}}(\mathrm{RH})/b_{\mathrm{scat,dry}}$ ratios and then differencing scattering at that RH and at the minimum RH. Equation (2) can then be solved at specific humidities using OLS regressions with or without an intercept (with or without residual water). It is emphasized that the resulting f(RH) curves are, except for the assumed dry mass scattering coefficients, based solely on measured data.

[59] Figure 7 is a plot of the f(RH) curves derived from the OLS analysis without an intercept term assuming e_s = 3.2 ± 0.4 m^2 g^{-1} and e_{oc} = 4.0 m^2 g^{-1} .The error bars represent the standard error of the regression coefficients, while the rectangle enclosing each error bar is associated with the standard deviation of the theoretically calculated dry mass scattering efficiencies (±0.4 m^2 g^{-1}) that are based on measured sulfate size distributions.

[60] The sulfate regression coefficient was significant at less than 1% at all humidities greater than 30%, while the regression coefficient associated with any other species was

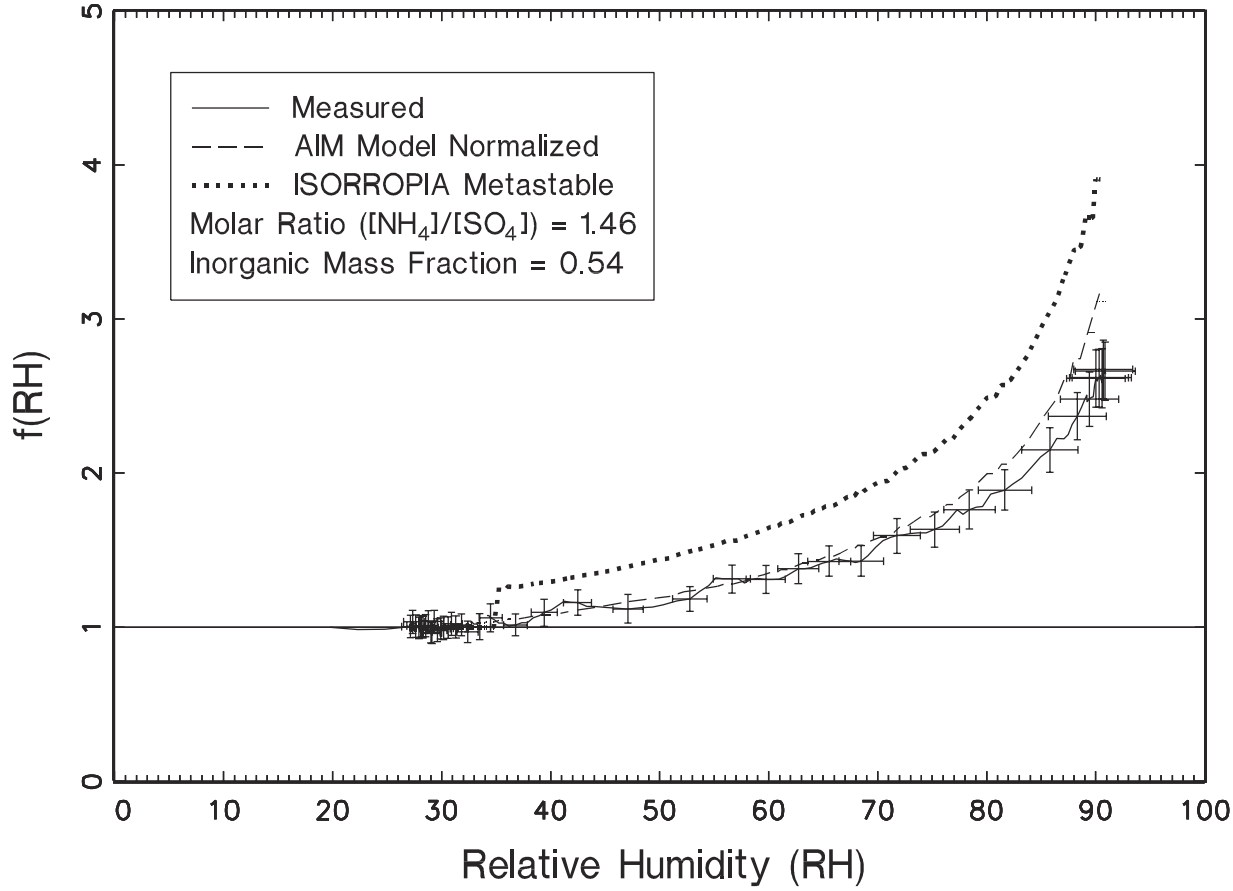

Figure 6. An example of measured *f*(RH) curve showing the overprediction of modeled *f*(RH) when it was assumed the aerosol was dry below 30% RH and the modeled *f*(RH) when it assumed an amount of water absorption predicted by the AIM equilibrium model at 30% RH. The molar ratio of ammonium to sulfate was 1.46 and the inorganic (SO_4 + NH_4 + NO_3 + Na) fine mass fraction was 0.54.

not statistically significant. Moreover, because the intercept term was not statistically different from zero, the results presented in Figure 7 were with a_0 set equal to zero. The R^2 values varied between a low of 0.14 at RH = 30% to above 0.80 for RH values above 50%. Even though the organic regression coefficients were not statistically significant, the implied organic *f*(RH) curve was included for reference. Notice that the average *f*(RH) data points shown in Figure 7 reflect some water absorption at 32% RH and possible deliquescence at about 45% RH and a second deliquescence point that occurred in the 75–80% range. The dotted line corresponds to the average *f*(RH) calculated directly from the AIM metastable growth curve while the solid line is the *f*(RH) normalized to 20%. The *f*(RH) curve, which is based on the normalized AIM metastable growth curve, approximates the statistically derived growth curve quite well.

[61] These results are consistent with the modeled *f*(RH) curves where good agreement between modeled and measured *f*(RH) was achieved by assuming organics did not absorb water and that on most days the aerosol contained some water at RHs in the 20–30% range. The water retention at these low RHs was consistent with the amount of water predicted by the AIM equilibrium model under conditions where solids were not allowed to form (metastable state). In the statistical model no prior assumptions were made about the hygroscopicity of various aerosol species. The analysis produced an *f*(RH) function for ammoniated sulfate that was nearly identical to the average *f*(RH) curve derived from the AIM metastable growth curves that were normalized to 20%

Table 10. Statistical Summary of the Percent Difference Between Modeled And Observed *f*(RH)

RH	Mean	Standard Deviation	Minimum	Maximum	*N*
20–25	1.37	3.33	−2.00	10.25	14
25–30	−0.48	3.03	−7.15	5.51	27
30–35	−0.51	3.42	−4.94	12.85	29
35–40	0.11	4.55	−6.64	18.07	29
40–45	−1.20	4.79	−7.78	16.87	29
45–50	−1.29	4.76	−7.97	15.28	29
50–55	−0.84	4.64	−7.04	15.50	29
55–60	−0.30	5.42	−11.36	18.02	29
60–65	0.44	3.50	−6.30	7.43	28
65–70	1.73	5.39	−10.30	16.08	29
70–75	2.32	6.03	−6.89	18.86	28
75–80	2.89	7.17	−8.19	19.98	27
80–85	3.82	10.00	−10.11	30.64	25
85–90	4.88	14.55	−12.15	43.07	20
90–95	−1.63	15.59	−17.24	36.33	15

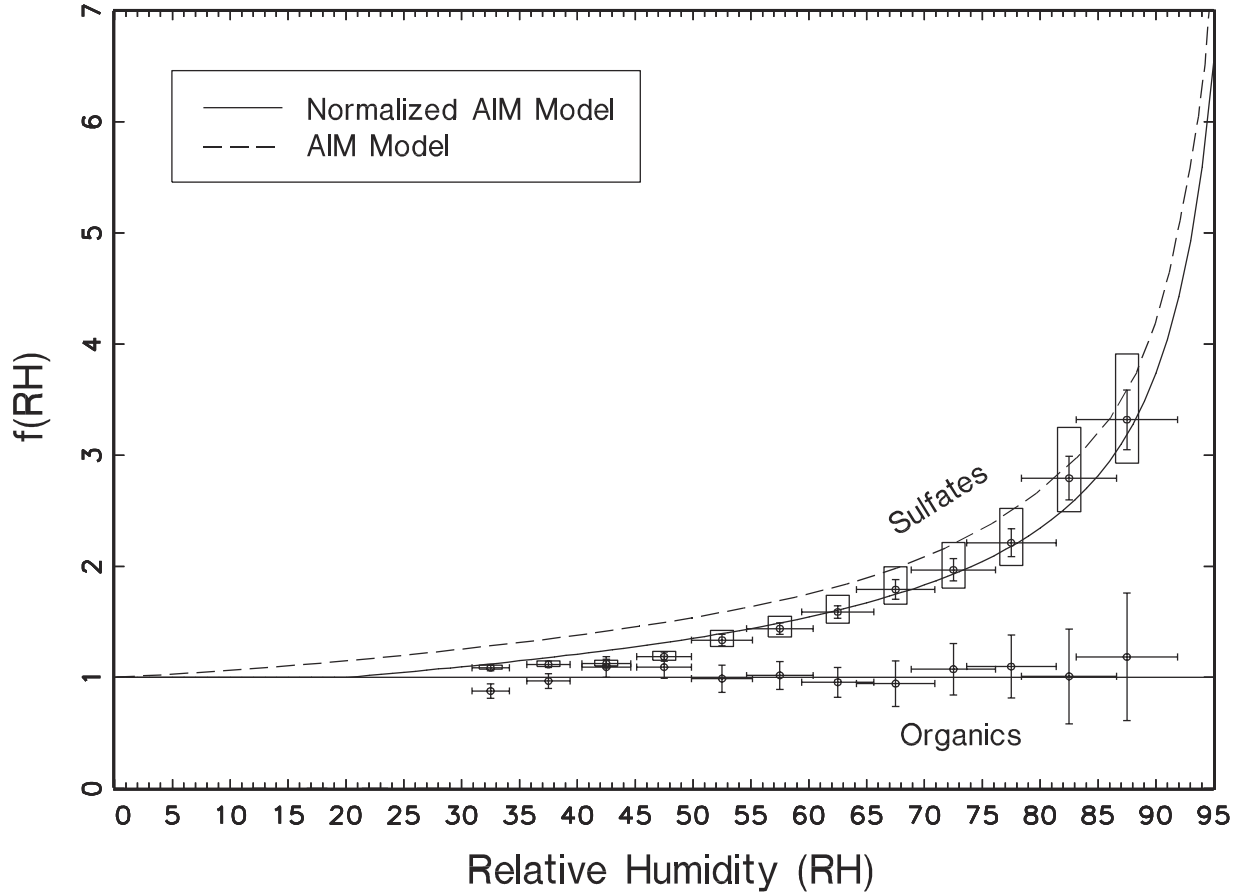

Figure 7. The f(RH) values for ammoniated sulfate and organics derived from a statistical model whose only input was measured scattering associated with absorbed water and ammoniated sulfate and organic mass concentrations. Also, shown for reference are the average f(RH) curves derived from the AIM equilibrium modeled metastable D/D_o curves without normalization and with normalization to 20% relative humidity.

RH(f(RH)normalized = f(RH)/f(20%)) and an f(RH) $\approx$ 1 for organics and soil).

10. Summary

[62] Gravimetric mass was measured and compared to mass reconstructed from the individual species, neglecting contributions from water associated with the aerosol. Measured gravimetric fine mass, defined to be the mass concentration of particles with aerodynamic diameters below 2.5 μm, was about 7% greater than reconstructed fine mass, with ammoniated sulfate contributing 51% of the mass and organics and soil contributing 21 and 22%, respectively. The R^2 between measured and reconstructed fine mass was 0.90. The fine mode consisted primarily of ammoniated sulfate, with an average ammonium to sulfate ratio of 1.52, and organics. The chemical composition of nitrates was found to be primarily in the form of sodium nitrate with some calcium nitrate and located in a coarse mode that was greater than about 1.0 μm. Only 3% of fine mass was associated with nitrates. On the 41 days where species size distributions were measured, the average mass mean diameter of ammoniated sulfate was 0.38 μm with a σ_g of 1.9.

[63] Dry and ambient scattering measurements were compared to modeled estimates of scattering that incorporated aerosol species concentrations, mass size distributions, and estimates of aerosol growth based on two equilibrium models. Dry mass scattering efficiencies of ammoniated sulfate varied from a low of 2.42 $m^2\ g^{-1}$ to a maximum of 4.06 $m^2\ g^{-1}$ with an average of 3.15 $m^2\ g^{-1}$. The lowest efficiencies occurred on the lowest-mass concentration days while the highest efficiencies corresponded to the highest-mass loadings. Accounting for varying sulfate ammoniation and changes in mass scattering efficiency over time, the average reconstructed dry scattering coefficient is 4% greater than measured and the R^2 between the two variables 0.93.

[64] Sulfate and nitrate f(RH) relative humidity factors, based on aerosol growth predicted by the AIM and ISORROPIA equilibrium models, were modeled for the deliquescent and metastable branches of the growth curves. These factors were used to estimate ambient reconstructed fine particle scattering. The use of the f(RH) curves associated with the ammoniated sulfate-AIM-metastable growth curves resulted in an average estimated fine particle scattering that was nearly equal (1% difference) to the average measured ambient scattering coefficient. The R^2 between

the measured and modeled scattering coefficient was 0.90. The use of the *f*(RH) curves associated with deliquescence growth curves resulted in an average under-prediction of modeled scattering by about 12% and a reduced correlation between the modeled and measured scattering coefficients. Contributions of nitrates to scattering were so low (<3.0%) that no conclusion could be drawn concerning the most appropriate nitrate *f*(RH) curves. The degraded fit between modeled and measured scattering associated with the use of deliquescence *f*(RH) curves suggest that aerosols were exposed to RHs greater than the deliquescence RH and were on the crystallization branch of the curve. In all cases *f*(RH) for organics was set equal to one.

[65] Assuming the best fit model, sulfates and organics were estimated to contribute 65.6 and 24.7% of fine particle ambient scattering while soil contributed 6.9% and nitrates contributed 2.9%. The difference between theoretical ambient and dry $PM_{2.5}$ scattering was about 19%, implying that despite the low study-average ambient RH of 44%, 19% of ambient scattering was associated with sulfate and nitrate water absorption. Nineteen percent was the same as the difference between the scattering coefficient measurements that were made by the ambient and dry $PM_{2.5}$ nephelometers.

[66] Finally, modeled estimations of *f*(RH) were compared to humidograph measurements that were made over a time period from Julian Days 238 to 301. Four general types of *f*(RH) curves were observed: deliquescence and crystallization behaviors, continuous growth from about 25 to 30% RH where the aerosol was apparently dry at the minimum RH, and continuous growth from 25 to 30% RH but where the aerosol retained water at the minimum RHs. There were five cases of each of the first three types of *f*(RH) curves and 29 of the last type. On days where deliquescence was observed, the modeled and measured deliquescence compared favorably (within a few RH points) on 2 days, while on 3 days the measured deliquescence point was more than 10% RH units below what the model predicted. On days when crystallization occurred, the modeled and measured crystallization points were within a few RH points of each other on all 5 days. The differences between average modeled and measured *f*(RH) curves above the crystallization or deliquescence points were 1 and 17%, respectively.

[67] Assuming the aerosol was dry at 25–30% RH represents a third case consisting of 5 sampling days. The measured and modeled curves agreed well above the deliquescence point; however, the measured curve below the deliquescence point fell between the modeled metastable and deliquescence curves. There were 29 measured *f*(RH) curves which again were continuous, with no clear crystallization or deliquescence, from approximately 1 to their respective maximum values. However, agreement between measured and modeled *f*(RH) is only achieved by assuming the AIM no-solids growth model where some water retention by the sulfate aerosol is indicated at relative humidities near the minimum RH, suggesting that the aerosol was not "dried out" at the beginning of the RH ramp. The *f*(RH) for organics and soil was set equal to 1 in all cases. The assumption that only inorganic species were hygroscopic was sufficient, to within the uncertainty of the measurement, to account for the measured increase in *f*(RH) as a function of RH. The average difference between measured and modeled *f*(RH) above 35% RH was on the order of 1%.

[68] The amount of scattering at a specific RH associated with individual species was also estimated using a statistical model where scattering associated with water retained on hygroscopic aerosols was regressed against individual species mass concentrations. The regression coefficients were shown to be proportional to the *f*(RH) curve associated with each individual aerosol species. It is emphasized that this approach relies only on measurements of the scattering coefficient and aerosol species mass concentrations and not on any assumptions concerning modeled growth or which species were hygroscopic. It was shown that, on the average, the *f*(RH) curve associated with sulfates was well predicted by the AIM no-solids growth estimation normalized to the RH at which the RH scan was initiated, implying that, on average, the sulfate aerosol retained water in the 25–30% RH range consistent with the AIM equilibrium model. The *f*(RH) curve for organics was not statistically different from one, while the regression coefficient associated with other species was not statistically significant.

[69] These results are consistent with our modeled *f*(RH) curves where good agreement between modeled and measured *f*(RH) was achieved by assuming organics did not absorb water and that on most days the aerosol retained some water at relative humidities in the 20–30% range. The water retention at these low relative humidities was consistent with the amount of water predicted by the AIM equilibrium model under conditions where solids were not allowed to form.

[70] **Acknowledgments.** Support for this BRAVO Study-related work was provided by the National Park Service. However, the results, findings, and conclusions expressed in this paper are solely those of the authors and are not necessarily endorsed by the management, sponsors, or collaborators of the BRAVO Study.

References

Air Resource Specialists, Inc., *Standard Operating Procedure and Technical Instructions for Nephelometer Systems*, *Rep. 4200-2000, 4100-3100*, Fort Collins, Colo., 1995.

Ansari, A. S., and S. N. Pandis, An analysis of four models predicting the partitioning of semivolatile inorganic aerosol components, *Aerosol Sci. Technol.*, *31*, 129–153, 1999.

Carrico, C. M., M. J. Rood, and J. A. Ogren, Aerosol light scattering properties at Cape Grim, Tasmania, during the First Aerosol Characterization Experiment (ACE 1), *J. Geophys. Res.*, *103*, 16,565–16,574, 1998.

Carrico, C. M., M. J. Rood, J. A. Ogren, C. Neusüß, A. Wiedensohler, and J. Heintzenberg, Aerosol optical properties at Sagres, Portugal, during ACE 2, *Tellus, Ser. B*, *52*, 694–716, 2000.

Chow, J. C., J. G. Watson, L. C. Pritchett, W. R. Pierson, C. A. Frazier, and R. G. Purcell, The DRI thermal/optical reflectance carbon analysis system: Description, evaluation, and applications in U.S. air quality studies, *Atmos. Environ. Part A*, *27*, 1185–1201, 1993.

Clegg, S. L., K. S. Pitzer, and P. Brimblecombe, Thermodynamics of multicomponent, miscible, ionic solutions, part II, Mixtures including unsymmetrical electrolytes, *J. Phys. Chem.*, *96*, 9470–9479, 1992.

Clegg, S. L., P. Brimblecombe, and A. S. Wexler, A thermodynamic model of the system $H^+ - NH_4^+ - SO_4^{2-} - NO_3 - H_2O$ at tropospheric temperatures, *J. Phys. Chem. A*, *102*, 2137–2154, 1998a.

Clegg, S. L., P. Brimblecombe, and A. S. Wexler, A thermodynamic model of the system $H^+ - NH_4^+ - Na^+ - SO_4^{2-} - NO_3 - Cl - H_2O$ at 298.15 K., *J. Phys. Chem. A*, *102*, 2155–2171, 1998b.

Cocker, D. R., N. E. Whitlock, R. C. Flagan, and J. H. Seinfeld, Hygroscopic properties of Pasadena, California aerosol, *Aerosol Sci. Technol.*, *35*, 637–647, 2001.

Covert, D. S., A. P. Waggoner, R. E. Weiss, N. C. Ahlquist, and R. J. Charlson, Atmospheric aerosols, humidity and visibility, in *Character and Origins of Smog Aerosols*, pp. 559–581, John Wiley, New York, 1979.

Day, D. E., W. C. Malm, and S. M. Kreidenweis, Aerosol light scattering measurements as a function of relative humidity, *J. Air Waste Manage. Assoc.*, *50*, 710–716, 2000.

Hand, J. L., S. M. Kreidenweis, D. Eli Sherman, J. L. Collett Jr., S. V. Hering, D. E. Day, and W. C. Malm, Aerosol size distributions and visibility estimates during the Big Bend Regional Aerosol Visibility and Observational Study (BRAVO), *Atmos. Environ.*, *36*, 5043–5055, 2002.

Malm, W. C., and D. E. Day, Optical properties of aerosols at Grand Canyon National Park, *Atmos. Environ.*, *34*, 3373–3391, 2000.

Malm, W. C., and D. E. Day, Estimates of aerosol species scattering characteristics as a function of relative humidity, *Atmos. Environ.*, *35*, 2845–2860, 2001.

Malm, W. C., and S. M. Kreidenweis, The effects of models of aerosol hygroscopicity on the apportionment of extinction, *Atmos. Environ.*, *31*, 1965–1976, 1997.

Malm, W. C., J. F. Sisler, D. Huffman, R. A. Eldred, and T. A. Cahill, Spatial and seasonal trends in particle concentration and optical extinction in the United States, *J. Geophys. Res.*, *99*, 1347–1370, 1994.

Malm, W. C., D. E. Day, and S. M. Kreidenweis, Light scattering characteristics of aerosols as a function of relative humidity, part I, A comparison of measured scattering and aerosol concentrations using the theoretical models, *J. Air Waste Manage. Assoc.*, *50*, 686–700, 2000a.

Malm, W. C., M. L. Pitchford, M. Scruggs, J. F. Sisler, R. B. Ames, S. Copeland, K. A. Gebhart, and D. E. Day, *Spatial and Seasonal Patterns and Temporal Variability of Haze and its Constituents in the United States: Rep. III*, Coop. Inst. for Res. in the Atmos., Fort Collins, Colo., 2000b.

Malm, W. C., B. A. Schichtel, R. B. Ames, and K. A. Gebhart, A ten-year spatial and temporal trend of sulfate across the United States, *J. Geophys. Res.*, *107*(D22), 4627, doi:10.1029/2002JD002107, 2002.

Marple, V. A., K. L. Rubow, and S. M. Behm, A microorifice uniform deposit impactor (MOUDI)—Description, calibration, and use, *Aerosol Sci. Technol.*, *14*, 434–446, 1991.

Molenar, J. V., Analysis of the real world performance of the Optec NGN-2 ambient nephelometers, in *Visual Air Quality: Aerosols and Global Radiation Balance*, pp. 243–265, Air and Waste Manage. Assoc., Pittsburgh, Pa., 1997.

Nenes, A., S. N. Pandis, and C. Pilinis, ISORROPIA: A new thermodynamic equilibrium model for multiphase multicomponent inorganic aerosols, *Aquat. Geochem.*, *4*, 123–152, 1998.

Ouimette, J. R., and R. C. Flagan, The extinction coefficient of multicomponent aerosols, *Atmos. Environ.*, *16*, 2405–2419, 1982.

Pitzer, K. S., and J. M. Simonson, Thermodynamics of multicomponent, miscible, ionic systems: Theory and equations, *J. Phys. Chem.*, *90*, 3005–3009, 1986.

Potukuchi, S., and A. S. Wexler, Identifying solid-aqueous phase transitions in atmospheric aerosol, I, Neutral-acidity solutions, *Atmos. Environ.*, *29*, 1663–1676, 1995a.

Potukuchi, S., and A. S. Wexler, Identifying solid-aqueous phase transitions in atmospheric aerosol, II, Acidic solutions, *Atmos. Environ.*, *29*, 3357–3364, 1995b.

Rood, M. J., M. A. Shaw, T. V. Larson, and D. S. Covert, Ubiquitous nature of ambient metastable aerosol, *Nature*, *337*(6207), 537–539, 1989.

Rotronic Instrument Corp., *Humidity-Temperature Meteorological Pro, MP-100F, Fact Sheet*, Rotronic Instrument Corp., Huntingdon, N. Y., 1998.

Saxena, P., and L. M. Hildemann, Water-soluble organics in atmospheric particles: A critical review of the literature and application of thermodynamics to identify candidate compounds, *J. Atmos. Chem.*, *24*, 57–109, 1996.

Sloane, C. S., Effect of composition on aerosol light scattering efficiencies, *Atmos. Environ.*, *20*, 1025–1037, 1986.

Trijonis, J. C., W. C. Malm, M. Pitchford, W. H. White, R. Charlson, and R. Husar, Visibility: Existing and historical conditions-causes and effects, in *State of Scientific Technology, Rep. 24*, Natl. Acid Precip. Assess. Program, Washington, D.C., 1990.

Turpin, B. J., and H. J. Lim, Species contribution to PM2.5 mass concentrations: Revisiting common assumptions for estimating organic mass, *Aerosol Sci. Technol.*, *35*, 602–610, 2001.

Virkkula, A., R. Van Dingenen, F. Raes, and J. Hjorth, Hygroscopic properties of aerosol formed by oxidation of limonene, alpha-pinene, and beta-pinene, *J. Geophys. Res.*, *104*, 3569–3579, 1999.

Waggoner, A. P., R. E. Weiss, and T. V. Larson, Insitu, rapid response measurement of $H_2SO_4/(NH_4)_2SO_4$ aerosols in urban Houston-A comparison with rural Virginia, *Atmos. Environ.*, *17*, 1723–1731, 1983.

White, W. H., and P. T. Roberts, On the nature and origins of visibility-reducing aerosols in the Los Angeles air basin, *Atmos. Environ.*, *11*, 803–812, 1977.

J. L. Collett, S. M. Kreidenweis, and T. Lee, Department of Atmospheric Science, Colorado State University, Fort Collins, CO 80523, USA.

D. E. Day, Cooperative Institute for Research in the Atmosphere (CIRA), Colorado State University, Fort Collins, CO 80523, USA.

W. C. Malm, National Park Service-Air Resources Division, Colorado State University/CIRA, Fort Collins, CO 80523, USA.